

## The Role of Thermal and Microstructural Parameters on Corrosion Resistance of Unsteady-State Horizontally Solidified Aluminum-Copper Hypoeutectic Alloys

Daniele L. Soares<sup>1,2</sup>, André S. Barros<sup>2</sup>, Marcelino Dias<sup>3</sup>, Antonio L. Moreira<sup>2</sup>, José C. Filho<sup>2</sup>, Adrina P. Silva<sup>2</sup>, Otávio L. Rocha<sup>1,2\*</sup>

<sup>1</sup> Federal Institute of Education, Science and Technology of Pará, IFPA, 66093-020, Belém, PA, Brazil

<sup>2</sup> Institute of Technology, Federal University of Pará, UFPA, 66075-110, Belém, PA, Brazil

<sup>3</sup> Department of Manufacturing and Materials Engineering, University of Campinas, UNICAMP, 13083-860, Campinas, SP, Brazil

\*E-mail: [otavio.rocha@ifpa.edu.br](mailto:otavio.rocha@ifpa.edu.br) or [otvocha@oi.com.br](mailto:otvocha@oi.com.br)

Received: 3 August 2016 / Accepted: 21 November 2016 / Published: 12 December 2016

---

This article analyzes the effects of Cu content, thermal and microstructural parameters on the mass loss and electrochemical corrosion resistance of two directionally solidified Al-XCu (X=3wt.% and 6wt.%) hypoeutectic alloys. The investigated solidification parameters include the growth rates ( $V_L$ ), cooling rates ( $T_R$ ), secondary dendrite arm spacings ( $\lambda_2$ ) and  $Al_2Cu$  intermetallic phase. Open circuit potential ( $E_{OC}$ ), anodic and cathodic polarization curves with the respective corrosion potential and current ( $E_{CORR}$  and  $I_{CORR}$ ) and  $H_2$  release volume evolution ( $H_2Vol$ ) corresponding to corrosion kinetics were used to study the corrosion resistance in a  $0.2 \text{ mol.L}^{-1}$  solution of HCl with an immersion time of 10 min at  $25 \text{ }^\circ\text{C}$ . The corrosion tests were performed at two different positions in relation to cooled interface of the studied alloys. It was found that the corrosion resistance is higher at position closer to the metal-mold interface, in which the  $V_L$  and  $T_R$  values are higher and the  $\lambda_2$  value is smaller. The results have shown, for both investigated alloys, that the  $Al_2Cu$  intermetallic particles are more susceptible to electrolytic corrosion for higher secondary dendrite arm spacings. On the other side, considering a same value for  $\lambda_2$  these particles are less resistant to corrosion in the eutectic matrix of the Al-3wt.%Cu alloy. Thus, the results have indicated that the Al-6wt.%Cu alloy has better electrochemical corrosion resistance than the Al-3wt.%Cu alloy.

---

**Keywords:** Al-Cu alloys; solidification; corrosion resistance; microstructure;  $Al_2Cu$  intermetallic particles

## 1. INTRODUCTION

The importance of aluminum alloys as material application in the aeronautics and automotive industries is due to its high electrical and thermal conductivities, high corrosion resistance, ease of fabrication but mainly due to its high strength-to weight ratio [1-19]. Among these alloys are those containing the alloying elements Cu, Mg and Si, e.g., commercial alloys of this type are those of the series 2011, 2014, 2017, 2018, 2124, 2219, 2319, 201.0, 203.0, 206.0, 224.0, and 242.0. In these series the Cu is the main alloying element, which forms with the aluminum an important stoichiometric compound, i.e., the  $Al_2Cu$  intermetallic phase, which is responsive for the high strength in family of 2xxx casting alloys [10-12,20,21].

The microstructure evolution during solidification depends on the process variables which can be divided into two groups, namely, those that describe the mold, and those that are related to the alloy. The mold is characterized by its size and geometry, temperature, and thermal properties while the alloy is characterized by its composition, temperature when it is poured, cooling rate, nucleation characteristics, transport of solute, melt convection, and heat-transfer coefficients at the metal/mold interface. During the solidification process of alloys the morphology most frequently observed is the dendritic which can be characterized by primary ( $\lambda_1$ ), secondary ( $\lambda_2$ ) and tertiary ( $\lambda_3$ ) dendrite arm spacings

Many studies [1-29] have analyzed the influence of thermal and microstructural variables of binary alloys on the mechanical properties and electrochemical corrosion, showing the role of dendritic arrays on the final properties. The main parameters studied in alloys are the temperature gradient ( $G_L$ ), solidification rate ( $V_L$ ), cooling rate ( $T_R$ ),  $\lambda_1$ ,  $\lambda_2$ , and  $\lambda_3$ . Some of these works have investigated the effects of these parameters on the corrosion resistance of aluminum-base alloys [10-12,14-17,29] and other metal alloy systems [21-28], all of them, however, developed for upward unidirectional solidification.

Concerning the  $\lambda_2$  effect on the corrosion resistance of metal alloys appears to be controversy in the literature. In an investigation [14] the correlation between ultimate tensile strength (UTS) and electrochemical corrosion resistance (ECR) during the upward unidirectional solidification involving Al-Cu and Al-Si alloys was examined experimentally. In the case of Al-5wt.%Cu alloy, it was observed that smaller  $\lambda_2$  values increase both UTS and ECR, however, for the Al-9wt.%Si alloy it was found that UTS increases and ECR decreases for these values. In addition, it was noted that pure aluminum is less susceptible to corrosion action than  $Al_2Cu$  intermetallic particles. It was also observed that the  $Al_2Cu$  particles were involved by the Al-rich phase in the eutectic mixture, which behaved as a protection against corrosion of the intermetallics. Ares et al. [21,22] have also studied the effects of thermal and structural parameters in resistance corrosion of Zn-Al alloys (ZA) and the authors describe in their results that when the grain size and  $\lambda_2$  increase ECR also increases, except for the ZA16 alloy.

Osório et al. [11] have performed experiments in order to examine ECR in two Al-Cu-Si alloys directionally solidified. The scale of the microstructure dendritic arrays and the solutes macrosegregation profiles have been examined. The authors have found that the impedance parameters and current density of the Al-8wt.%Cu-3wt.%Si alloy have better ECR than the Al-6wt.%Cu-1wt.%Si

alloy, independently of the scale of the dendrite arm spacings. On the other side, taking into account the Cu macrosegregation region, it was observed that  $I_{CORR}$  decreased to small values of  $\lambda_2$ . In another article [12], on as-cast Al-Cu-Si alloys, Osório et al. have concluded that the Cu content is the driving-force leading to a decrease in the corrosion resistance.

Regarding the role of Cu-based intermetallic particles in the ECR Osório et al. [10] have developed a study in order to investigate the influence of  $Cu_6Sn_5$ ,  $Ti_2Cu$ , and  $Al_2Cu$  intermetallics on pitting corrosion of three different as-cast alloys: Al-5wt.%Cu, Ti-5wt.%Cu, and Sn-2.8wt.%Cu. The authors have observed that the lamellar morphology produced by alternated solvent-rich/intermetallics phases, which features the microstructure of analyzed alloys, furnishes an enveloping effect forming a protective barrier against ECR. It was observed the authors that  $Al_2Cu$  particles are more sensitive to the effects of ECR than pure aluminum.

In this sense, the aim of this work is to examine the effects of the Cu content,  $V_L$ ,  $T_R$ , and  $\lambda_2$  in ECR of two unsteady-state horizontally solidified Al-XCu (X=3wt.% and 6wt.%) hypoeutectic alloys. To achieve the objectives the technical procedures of open-circuit potential, polarization curves and hydrogen gas evolution were used.

## 2. EXPERIMENTAL PROCEDURE

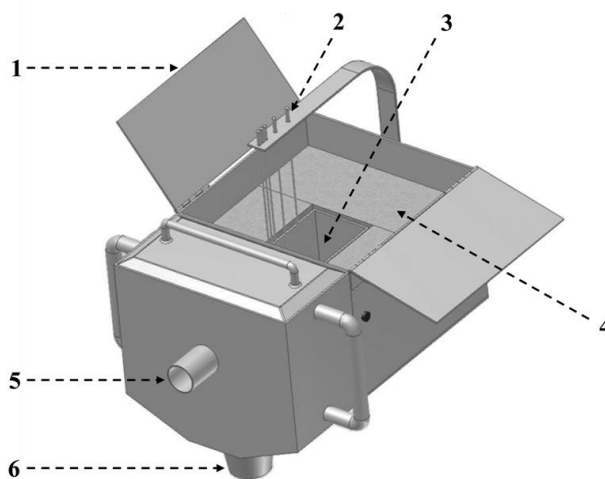


**Figure 1.** The casting assembly used in directional solidification experiments. (1) Setup cover, (2) thermocouples, (3) stainless steel mold (inner wall), (4), insulating ceramic, shielding, (5) water inlet, (6) water outlet.

Fig. 1 shows the water-cooled experimental device used for horizontal directional solidification of the Al-3wt.% Cu and Al-6wt.%Cu alloys. The alloys were melted and poured (starting melt superheats in 10% above *liquidus* temperature) in a stainless steel mold which was 60 mm high, 70 mm wide, 110 mm long, and 3 mm thick. The upper part of the mold was closed with refractory material and the lateral inner mold walls were protected with alumina to avoid heat losses. The experimental device was projected in such a way that the heat could be extracted only through a water-cooled system located at the metal-mold interface with water flow constant of 12 LMP, making

possible horizontal directional solidification. More details about the casting assembly used in experiments can be found in a previous article [18].

In order to determine  $V_L$  and  $T_R$ , temperature measurements were obtained during the solidification process for each alloy via output of a set of type K thermocouples sheathed in 1.6 mm diameter steel tubes located in different positions from metal-mold interface, as indicated in Fig. 1, which were linked to a data acquisition system connected to a computer.

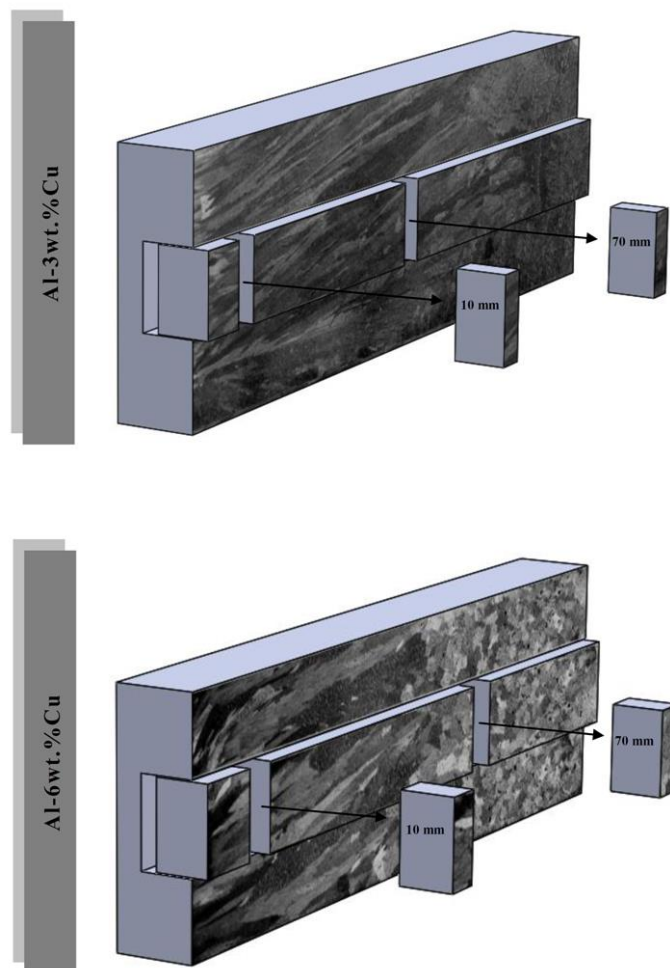


**Figure 2.** Removal of the cast ingot samples for the electrochemical corrosion and mass loss tests.

The ingots resulting from the horizontal directional solidification process were sectioned along its longitudinal axis, which is parallel to the direction of the heat flow extracted from the mold. In order to reveal the macrostructures, the metallographic samples were polished with abrasive papers and then etched, during approximately 10 minutes, with an acid solution composed of  $H_2O$  (5 ml),  $HF$  (5 ml),  $HNO_3$  (30 ml), and  $HCl$  (60 ml). After this, selected longitudinal sections of the ingot were both polished and etched with  $NaOH$  5% to quantify and characterize the dendritic structure. The  $\lambda_2$  were measured taking into account the average distance between adjacent side branches on longitudinal sections of  $\lambda_1$  stalks [4,5,8,9]. Al-Cu alloys were used as the working electrode removed from as cast ingots in the positions 10 mm and 70 mm in relation to the metal-mold interface, with dimensions of 15x10x2 mm as shown in Fig. 2.

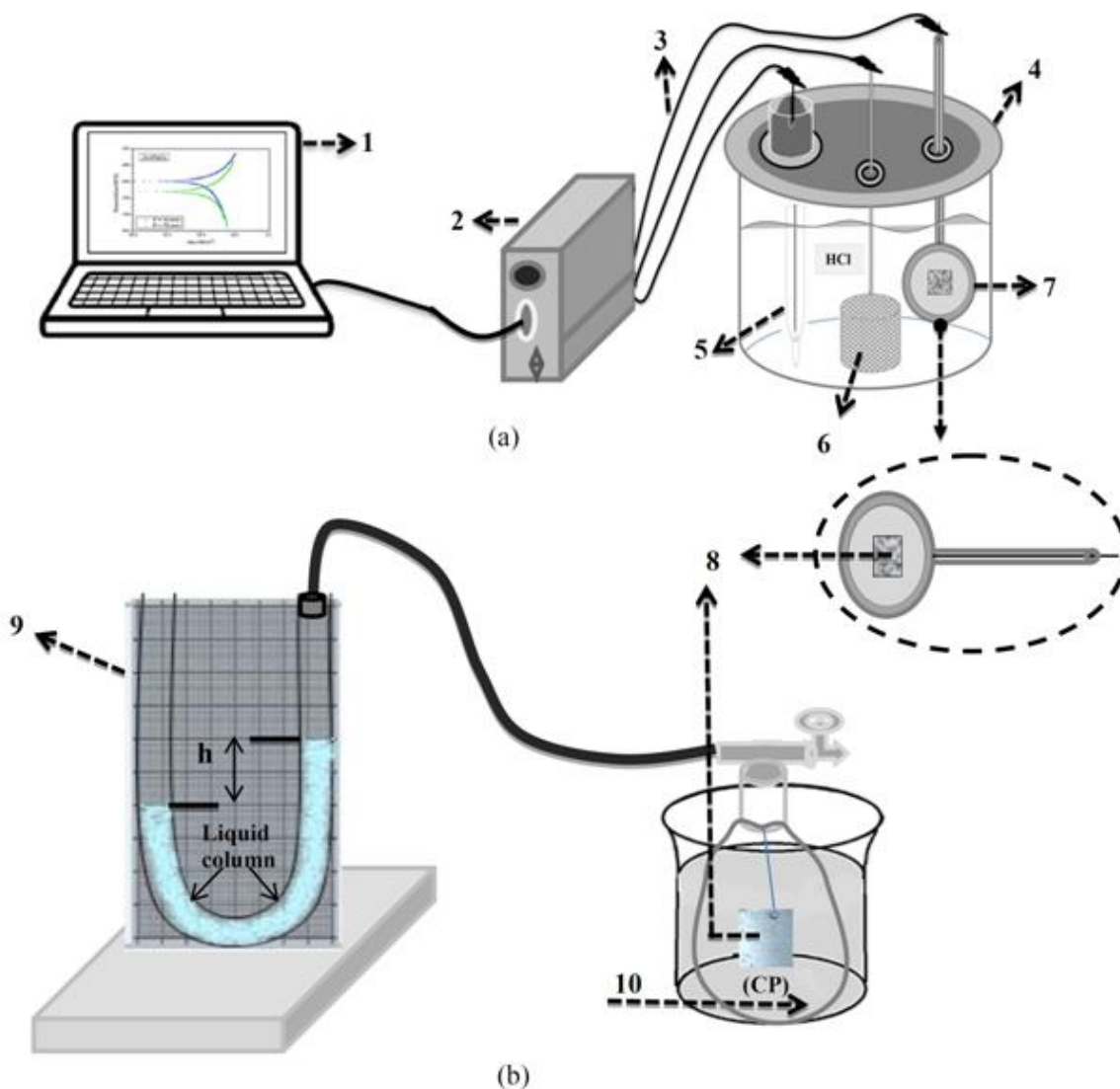


**Figure 3.** Illustrative drawings showing the tests: (a) electrochemical corrosion, and (b) mass loss. (1) Computer, (2) potentiostat/galvanostat, (3) electric connectors, (4) electrochemical cell, (5) reference electrode - saturated calomel electrode (SCE), (6) auxiliary electrode of large area (Pt), (7) working electrode (WE), (8) as-cast ingot sample, (9) U-tube manometer, (10) electrolyte of HCl.

The investigated samples were used in open-circuit potential, polarization curves and hydrogen gas evolution. Before each experiment, the surface of Al-Cu samples were worn by 220, 420, and 600-grades emery papers. After this, the samples were rinsed with ethanol and washed with distilled water. Measurements were performed in aerated solution of HCl ( $0.2 \text{ mol L}^{-1}$  at  $25 \text{ }^\circ\text{C}$ ) and the equipment used in electrochemical tests was a potentiostat of Ganry Instruments. A saturated calomel electrode and pt grid were used, respectively, as reference and auxiliary electrodes. Besides, they were performed at least three measurements for each fresh polished sample in order to verify the reproducibility of the electrochemical test. Fig.3 shows the schematic design of the corrosion testing

device, with items 1 to 7 refer to the electrochemical testing and 8 to 10 to the of hydrogen gas evolution.

### 3. RESULTS AND DISCUSSION

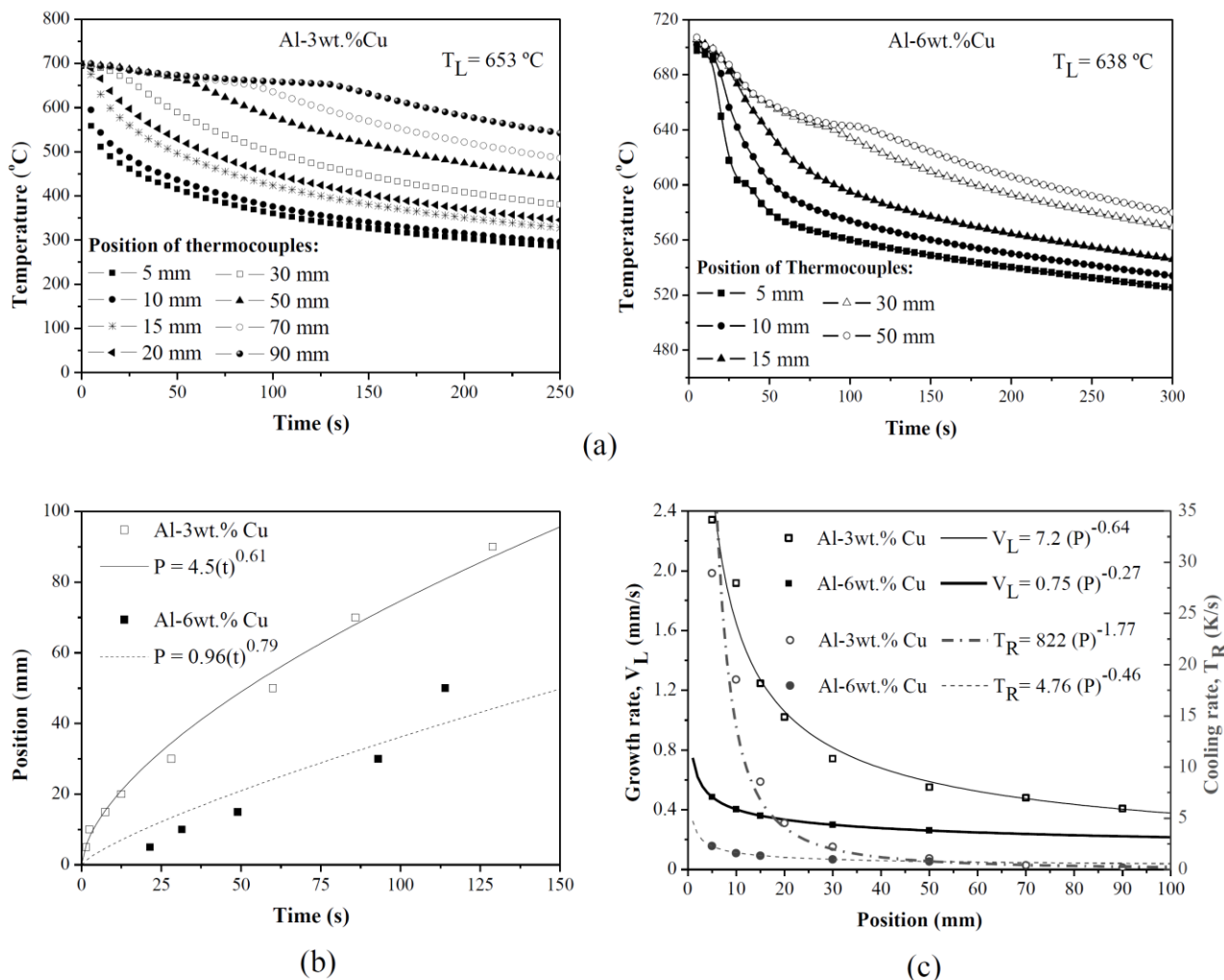


**Figure 4.** Experimental results of the thermal analysis for the alloys investigated in this study: (a) cooling curves; (b) position of the *liquidus* isotherms as a function of time and (c) growth rate and cooling rate as functions of the *liquidus* isotherm position.

Experimental cooling curves of the examined alloys are shown in Fig. 4a. In order to calculate the movement of the *liquidus* isotherm, a plot of position from the metal-mold interface as a function of time, whose experimental results for both investigated alloys are shown in Figs. 4b and 4c. The results presented in Fig. 4b show the solidification front (*liquidus* isotherm) of Al-3wt.%Cu alloy advancing faster than that of Al-6wt.%Cu alloy, whose behavior reflects on the  $V_L$  and  $T_R$  values which are higher for the Al-3wt.%Cu alloy, as shown by the curves and equations within the Fig.4c. It was evidenced for Al-3wt.%Cu alloy that the  $V_L$  and  $T_R$  values ranged from 0.47 mm/s to 1.65 mm/s

and 0.44 K/s to 14 K/s and for Al-6wt.%Cu alloy from 0.24 mm/s to 0.40 mm/s and 0.67 K/s to 1.65 K/s, respectively.

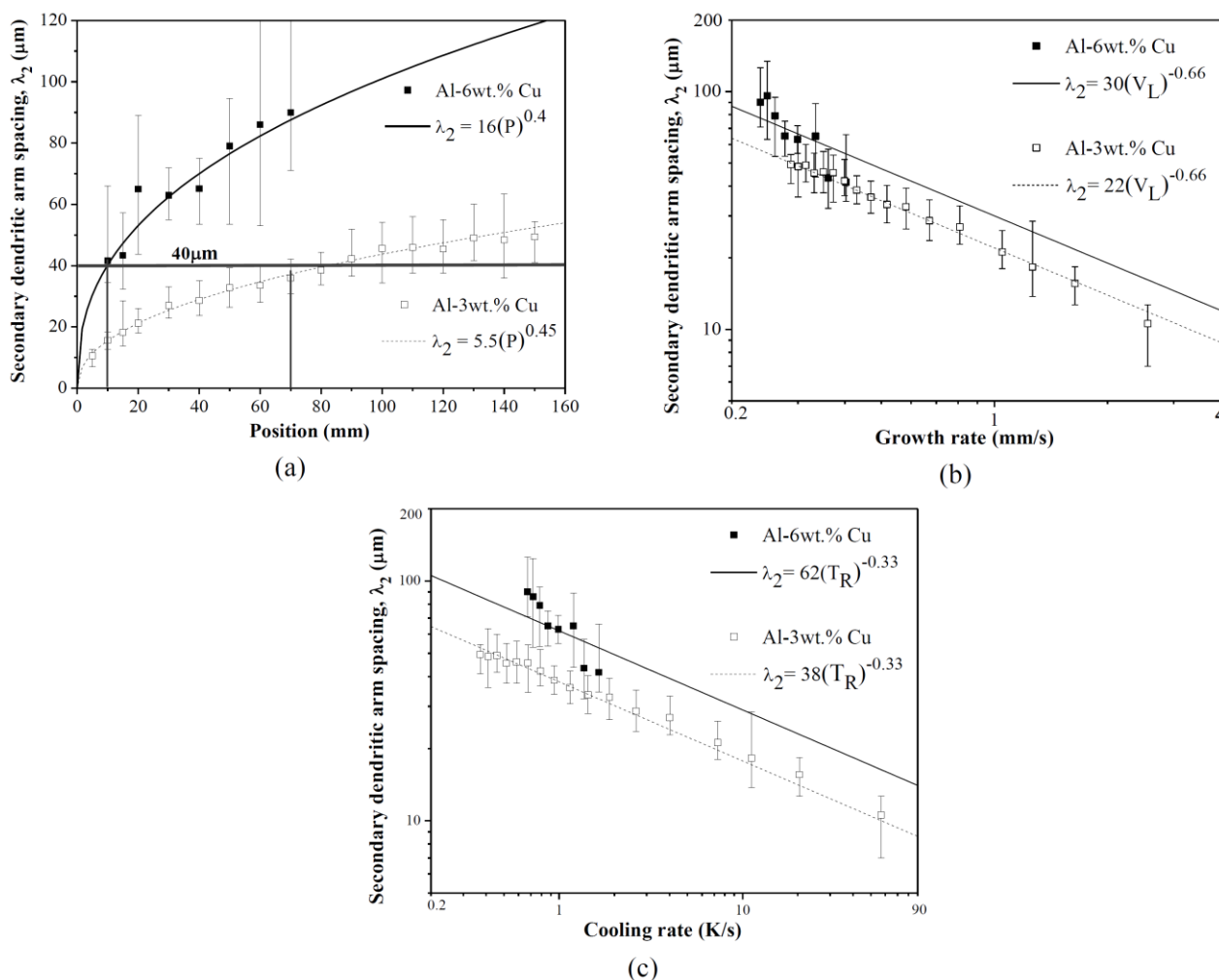


**Figure 5.** Correlation between secondary dendrite arm spacing as a function of: (a) position of the liquidus isotherm, (b) growth rate and (c) cooling rate, for both investigated alloys.

It is well known that  $V_L$  and  $T_R$  exert influence on  $\lambda_2$  and so in this work these thermal parameters were interrelated with  $\lambda_2$ , whose results are shown in Fig. 5, for both investigated alloys. It can be observed that power-type mathematical expressions, represented by  $\lambda_2 = \text{Constant} (V_L)^{-2/3}$  and  $\lambda_2 = \text{Constant} (T_R)^{-1/3}$ , featuring the experimental growth laws of  $\lambda_2$  as a function of  $V_L$  and  $T_R$ , respectively. These results are consistent with the predicted exponents in the mathematical equation of Bouchard-Kirkaldy’s theoretical model [20] as well as with the experimental observations reported by Rocha et al. [8] and Peres et al. [9]. It is known that  $\lambda_2$  decreases with increasing solute content [4,8,9,20], however, it can be seen in Fig. 5 that smaller  $\lambda_2$  values were reached for the Al-3wt.%Cu alloy, whose behavior can be explained by the high cooling rates for this alloy. This can be confirmed by fixing  $\lambda_2 = 40 \mu\text{m}$  on the ordinate axis of the graphs  $\lambda_2 = f(P)$  shown in Fig. 5, in a which can be noted that due to the high cooling rates achieved by the horizontal solidification of the Al 3wt.%Cu

alloy the fixed  $\lambda_2$  value (40  $\mu\text{m}$ ) was reached at the position 70 mm from the metal-mold interface. On the other hand, for the Al-6wt.%Cu alloy, due to the low cooling rates, the same  $\lambda_2$  value is as soon verified at position 10 mm.

Typical microstructures resulting of the horizontal solidification process for three positions from the cooled interface are shown in Fig. 6. It is confirmed by the dendritic microstructures the effect of  $V_L$  and  $T_R$  on  $\lambda_2$  values, i.e., it can be observed the coarsening of dendrite arms with the advancement of the solidification.

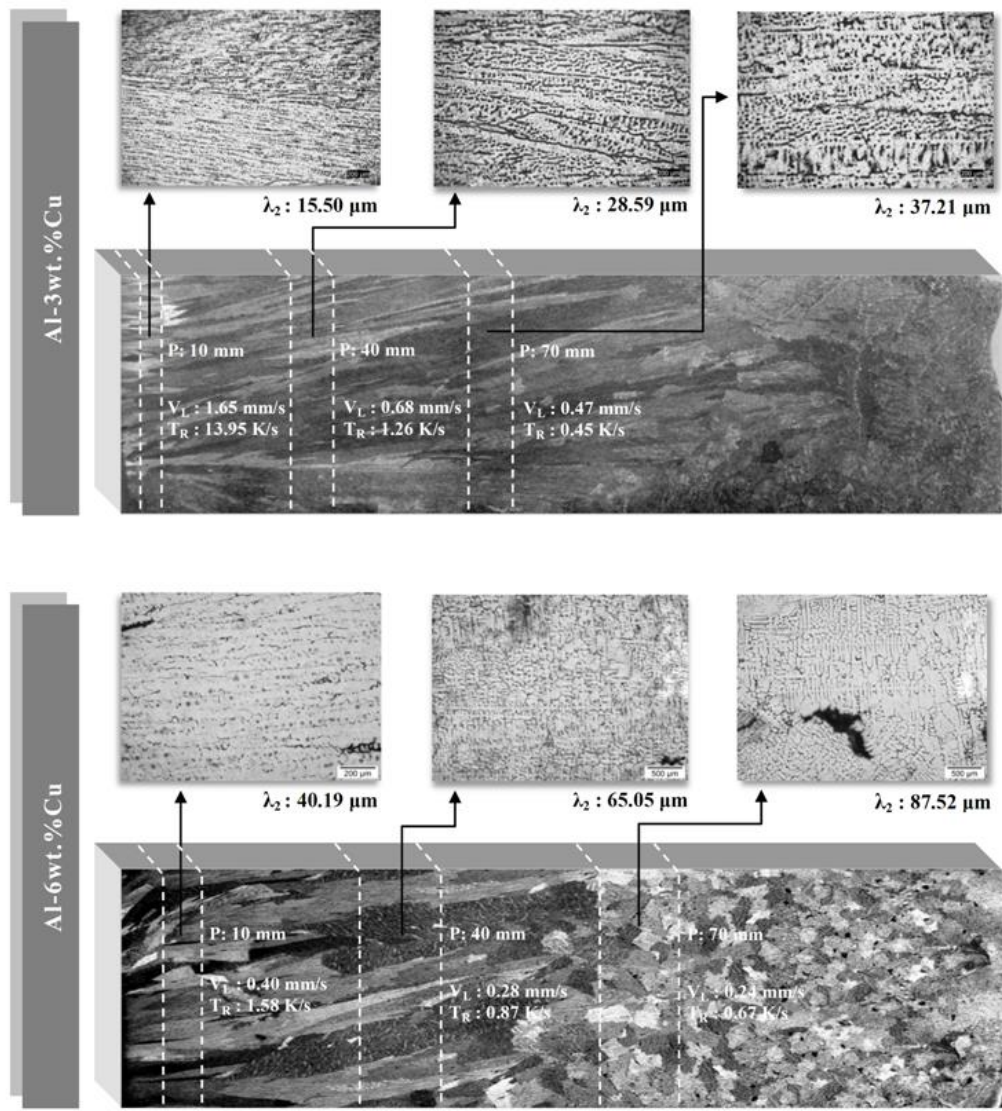


**Figure 6.** Solidification microstructures analyzed alloys in this work Al-3wt.%Cu and Al-6wt.%Cu alloys.

With the purpose of examining the effects of  $V_L$ ,  $T_R$  and  $\lambda_2$  in ECR two samples of as-cast ingots of both investigated alloys were extracted in 10 mm and 70 mm positions in relation the cooled interface. Figs. 7 and 8 show, for both studied alloys, measurements of the open circuit potential ( $E_{OC}$ ) and the respective polarization curves, corresponding to (both) positions from the metal-mold

interface, in HCl electrolyte solution ( $0.2 \text{ mol.L}^{-1}$   $25 \text{ }^\circ\text{C}$ ) with a time of 10 minutes. Concerning the behavior of the  $E_{OC}$ , it can be seen in Figs. 7a e 8a in both cases an increase in  $E_{OC}$  values at the beginning of electrolytic corrosion test, which are stabilized after a time interval. It is found at position 10 mm for the Al-3wt.%Cu alloy, an increase in  $E_{OC}$  values to 150 s, and after this time interval occurs stabilization of the  $E_{OC}$  in an approximate value of  $E_{OC} \cong -672 \text{ mV/SCE}$  for higher time. This is observed for the position 70 mm (Fig.7a) that the  $E_{OC}$  values increased to 50 s, maintaining constant after this time interval, resulting in approximately  $E_{OC} \cong -693 \text{ mV/SCE}$ . Regarding the behavior of Al-6wt.%Cu alloy it was verified that the  $E_{OC}$  values increased to 25 s and 75 s at positions 10 mm and 70 mm, and that after these time intervals the  $E_{OC}$  values remain constant at approximately  $E_{OC} \cong -666 \text{ mV/SCE}$  and  $E_{OC} \cong -688 \text{ mV/SCE}$ , respectively.

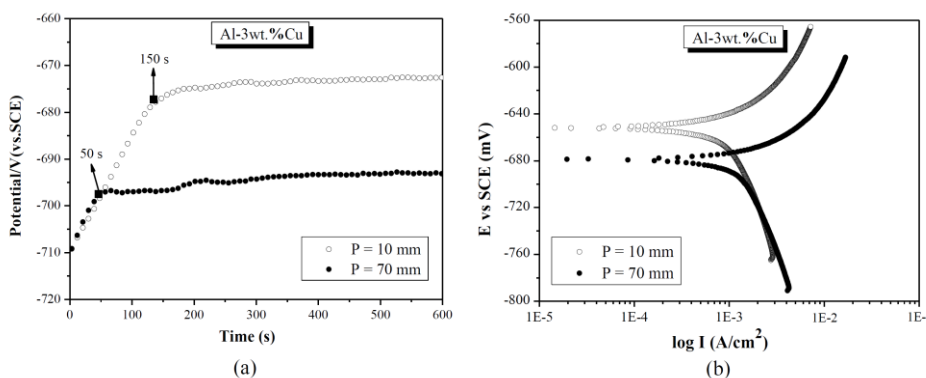


**Figure 7.** Experimental curves obtained for Al-3wt%Cu alloy in  $0.2 \text{ mol.L}^{-1}$  HCl solution at positions 10 mm and 70 mm from the metal/mold interface. (a) Open circuit potential- $E_{oc}$  and (b) Polarization.

In Figs.7b and 8b are presented the anodic and cathodic polarization curves obtained in HCl ( $0.2 \text{ mol L}^{-1}$  to  $25 \text{ }^\circ\text{C}$ ) at positions 10 mm and 70 mm for both investigated alloys. It can be noted that these respective curves for  $P = 10 \text{ mm}$  in both cases have a behavior more anodic when compared with those obtained at the position 70 mm. This can be interrelated to the observed behaviors of open circuit potential shown by Figs. 7a and 8a.

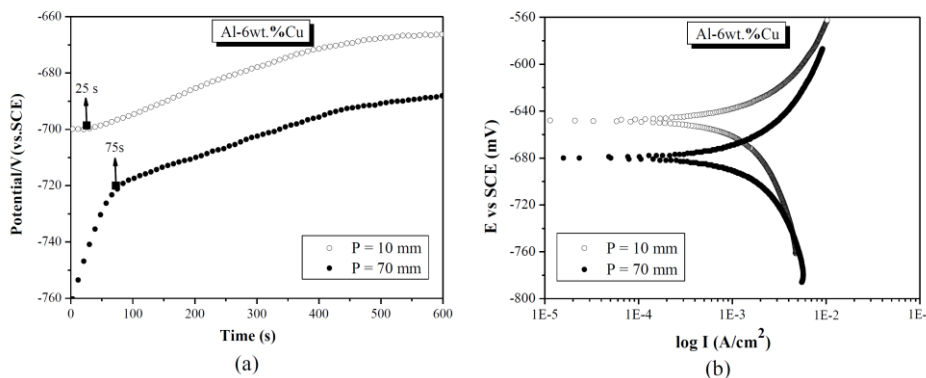


**Figure 8.** Experimental curves obtained for Al-6wt.%Cu alloy in  $0.2 \text{ mol.L}^{-1}$  HCl solution at positions 10 mm and 70 mm from the metal/mold interface. (a) Open circuit potential- $E_{oc}$  and (b) Polarization.

The corrosion potential ( $E_{CORR}$ ), corrosion current density ( $I_{CORR}$ ), anodic Tafel slope ( $\beta_a$ ) and cathodic Tafel slope ( $\beta_c$ ) values were calculated from the polarization curves for both investigated positions, using the method of Tafel-curve extrapolation [29, 30], and the results interconnected with  $V_L$ ,  $T_R$  and  $\lambda_2$  values are shown in Tab. 1. According to Fig. 4c, higher values of both growth rates and cooling rates are obtained near the cooled surface. Then, a decreasing curve along the ingot can be observed due to the increasing thermal resistance of the solidified thickness with distance from the metal-mold interface. This behavior reflects on the  $\lambda_2$  experimental values (Fig. 5). In this sense, it can be seen by Tab. 1, for the investigated alloys in this work, that  $I_{CORR}$  is estimated from slopes ( $\beta_a$  and  $\beta_c$ ) of the linear parts of the curves of Figs. 7b and 8b. Inspection of the polarization curves reveals that  $\beta_a$ ,  $\beta_c$  and  $I_{CORR}$  are reduced, with decreasing of  $\lambda_2$ . This behavior indicates that dendritic structures with lower secondary dendrite arm spacings have higher corrosion resistance.

**Table 1.** The electrochemical parameters of alloys investigated, in 0.2 mol.L<sup>-1</sup> solution of HCl.

Alloy	Position from the cooled interface (mm)	$V_L$ , $T_R$ , and $\lambda_2$	$E_{CORR}$ (mV/SCE)	$I_{CORR}$ ( $\mu\text{A}/\text{cm}^2$ )	$\beta_a$ (mV/decade)	$-\beta_c$ (mV/decade)
Al-3wt.%Cu	10	1.65 mm/s 13.95 K/s 15.50 $\mu\text{m}$	-665.5	56.98	35	93
	70	0.47 mm/s 0.45 K/s 37.21 $\mu\text{m}$	-692.8	140.74	58	102
Al-6wt.%Cu	10	0.40 mm/s 1.58 K/s 40.19 $\mu\text{m}$	-663.9	66.99	38	95
	70	0.24 mm/s 0.67 K/s 87.52 $\mu\text{m}$	-688.79	110.0	63	114

In the present study the ECR was also analyzed by hydrogen released volume evolution measured ( $H_2\text{Vol}$ ) at positions 10 mm and 70 mm from the cooled interface, whose results are shown in Fig. 9. It is possible to evidence a low  $H_2$  release volume in the first 20 minutes of test, independently of Cu content and position. This behavior can be attributed to the  $Al_2O_3$  layer formation on the surface of the as-cast samples, which can be acting simultaneously as protective and  $H_2$  reaction inhibitor layers (cathodic). It is also observed that after the time of 20 minutes the  $H_2$  release volume increases more rapidly for the position of 70 mm, providing higher corrosion rate at this position. In this sense, parameterizing the time of 90 minutes (final of test) in the curves corresponding to Figs. 9a and 9b, it was possible to determine the  $H_2$  released volumes maximum values, resulting at positions 10 mm and 70 mm the values of 185.21 mm<sup>3</sup>/cm<sup>2</sup> and 271 mm<sup>3</sup>H<sub>2</sub>/cm<sup>2</sup> for the Al-3wt.%Cu alloy and 95.8 mm<sup>3</sup>H<sub>2</sub>/cm<sup>2</sup> and 225.47 mm<sup>3</sup>H<sub>2</sub>/cm<sup>2</sup> for Al-6wt.%Cu alloy, respectively, which allow to confirm that  $H_2$  higher volumes are released at 70 mm position, so higher mass loss was found to occur at this position.

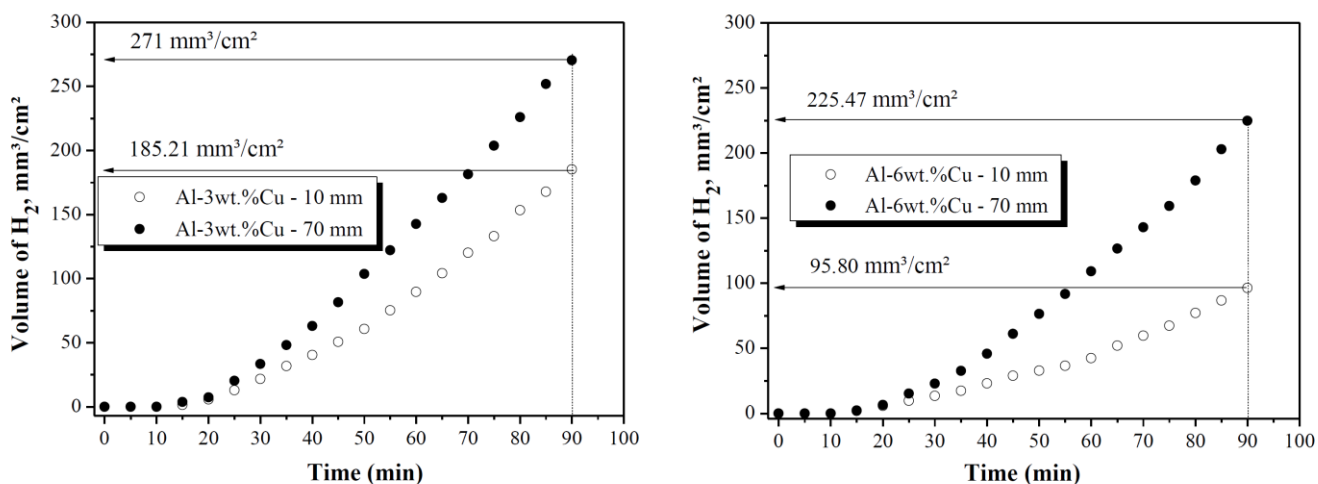


**Figure 9.** Experimental results of H<sub>2</sub> evolution measures in positions 10 mm and 70 mm from the metal/mold interface of both investigated Al-Cu alloys in 0.2 mol.L<sup>-1</sup> HCl solution.

**Table 2.** Experimental rate values of H<sub>2</sub> released volume during the electrochemical test for both investigated Al-Cu alloys.

Alloy	d(H <sub>2</sub> Vol)/dt (mm <sup>3</sup> .cm <sup>-2</sup> )	
	10 mm from the cooled interface	70 mm from the cooled interface
Al-3wt.%Cu	2.6	3.8
Al-6wt.%Cu	1.3	3.1

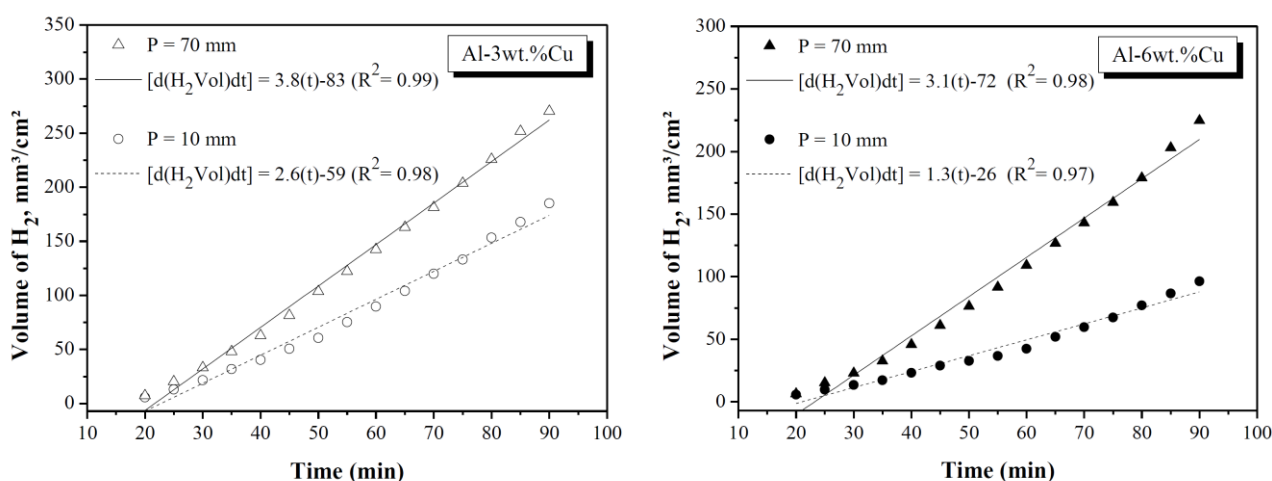


**Figure 10.** Linearized H<sub>2</sub> release evolution curves for both position of the investigated alloys in 0.2 mol.L<sup>-1</sup> HCl solution.

The H<sub>2</sub> rate released total volume was calculated by linearization of H<sub>2</sub> release volume evolution curves (H<sub>2</sub>Vol), shown in Fig. 9, from the stabilization time which in this case was 20

minutes. Thus, linearized new curves of H<sub>2</sub> release volume evolution were plotted, whose values are the same shown in Figs. 9a and 9b. The time interval between 20 to 90 minutes which represents the effective variation of H<sub>2</sub> release volume evolution. Fig.10 shows the linearized curves and the "fit" of the linear equations obtained for the positions 10 mm and 70 mm. The final values of this rate are resulting of the linear equations from the curves shown in Figs. 10a and 10b, i.e., [d(H<sub>2</sub>Vol)/dt], whose values are consolidated in Tab. 2. It is evidenced that H<sub>2</sub> higher release volume rate values [d(H<sub>2</sub>Vol)/dt] were found at position 70 mm, confirming lower ECR at this position.

With the view to investigate the effect of solute content on the ECR of the studied alloys, in this work the open circuit potential as a function of time, polarization as a function of current density, and of H<sub>2</sub> release volume evolution as a function of time profiles were plotted for a λ<sub>2</sub> constant value equal to 40 μm. The positions from the cooled lateral interface were 10 mm and 70 mm for Al-6wt.%Cu and Al-3wt.%Cu alloys, respectively (Fig. 6). The behavior of both profiles is shown in Figs. 11a and 11b in which can be seen that the E<sub>OC</sub> and polarization profiles exhibit more anodic characteristics for the Al-6wt.%Cu alloy. Consequently, this alloy releases less H<sub>2</sub> volume than Al-3wt.%Cu alloy, as observations in Figs 11c and 11d. It can be verified, therefore, that Al-6wt.%Cu alloy presents higher ECR than the Al-3wt.%Cu alloy.

Microstructures were characterized after the corrosion tests. Figs.12 and 13 show micrographs revealed by Scanning Electron Microscopy (SEM) and the corresponding microanalysis by EDS/SEM for both investigated positions in Al-Cu alloys. It is noted, in SEM micrographs, the presence of aluminum rich matrix (α-Al) as well as the Al<sub>2</sub>Cu intermetallic phase. It is observed in Fig. 12 that the Al<sub>2</sub>Cu particles have a greater corrosion action at position of 70 mm, in which V<sub>L</sub> and T<sub>R</sub> are smaller and consequently the λ<sub>2</sub> value is higher.

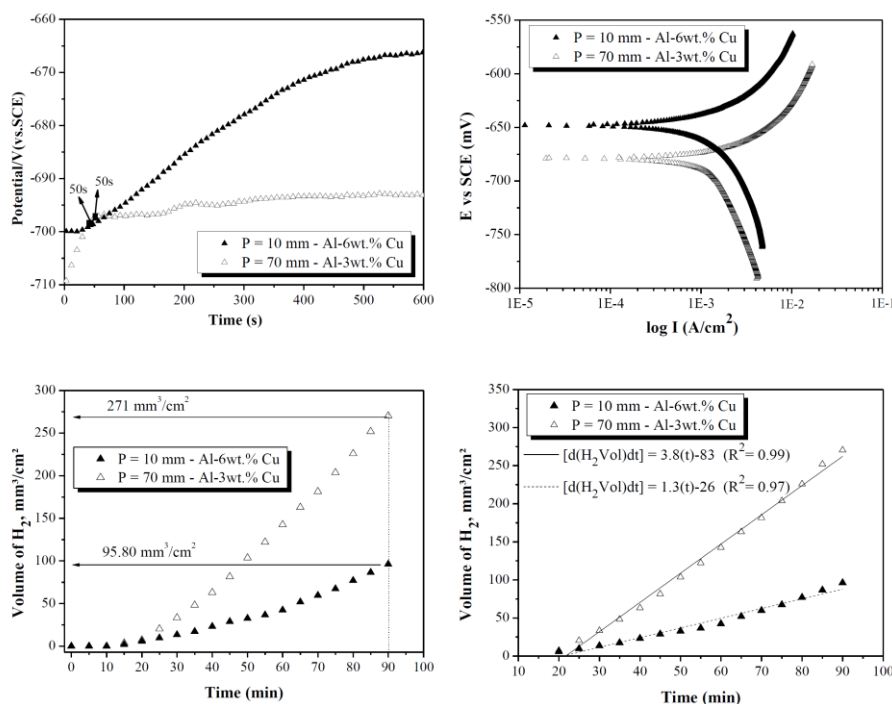


**Figure 11.** Open circuit potential and polarization curves and H<sub>2</sub> release volume evolution, for λ<sub>2</sub> = 40 μm.

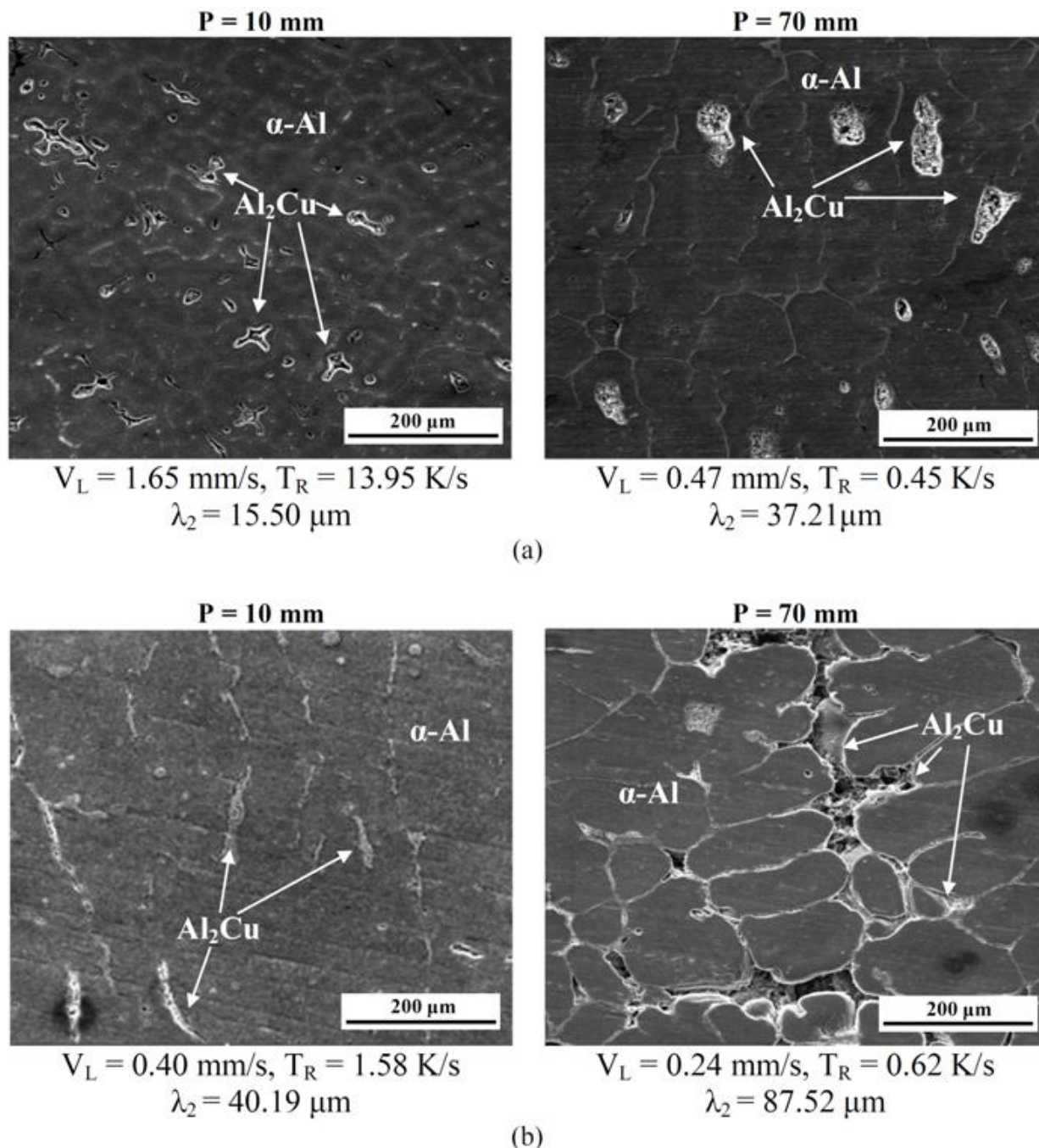


**Figure 12.** Micrographs obtained by scanning electron microscopy (SEM) for both the analyzed positions of the investigated alloys: (a) Al-3wt.%Cu alloy and (b) Al-6wt.%Cu alloys.

Concerning the effect of Cu content for a  $\lambda_2$  constant value, in Fig. 13 are presented microanalysis performed at positions 70 mm and 10 mm of Al-3wt.%Cu and Al-6wt.%Cu alloys, respectively, whose positions have occurred  $\lambda_2 = 40 \mu\text{m}$ . It is evidenced that for a  $\lambda_2$  constant value the  $\text{Al}_2\text{Cu}$  particles are more sensitive to corrosion activity in Al-3wt.%Cu that in Al-6wt.%Cu alloy.

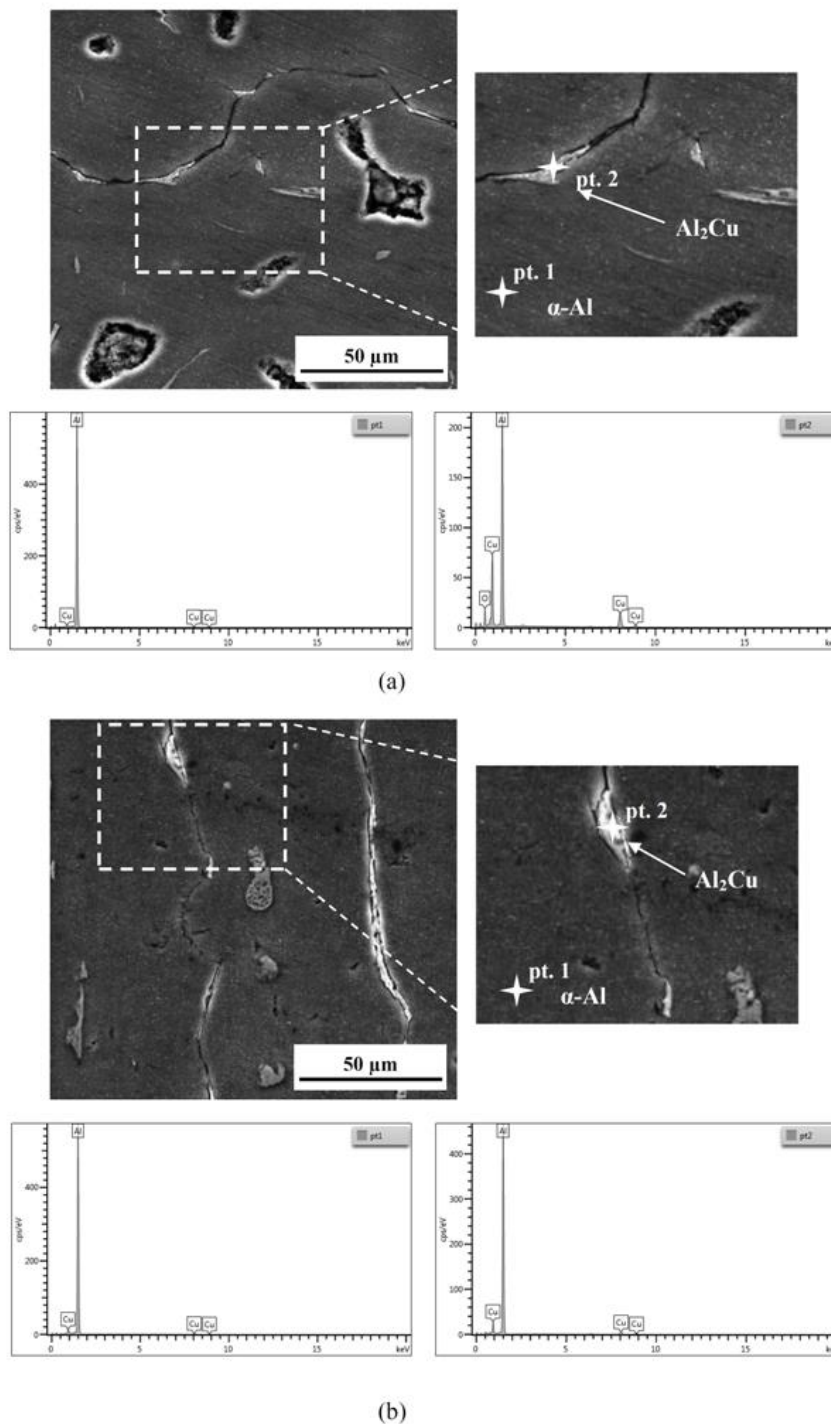


**Figure 13.** Microanalysis EDS/SEM of both the investigated alloys for  $\lambda_2 = 40\mu\text{m}$ : (a) Al-3wt.%Cu alloy at P = 70 mm from the cooled interface and (b) Al-6wt.%Cu alloy at P = 10 mm from the cooled interface.

#### 4. CONCLUSIONS

An experimental study was performed in order to analyze the effects of Cu content, solidification thermal variables, and structural parameters on ECR of transient directionally solidified Al-Cu hypoeutectic alloys. The main conclusions are as follows:

1. It was found that the solidification kinetics was faster for Al-3wt.%Cu alloy and, consequently, the  $V_L$  and  $T_R$  experimental values have ranged between 0.24 mm/s and 0.40 mm/s as well as 0.67 K/s and 1,65 K/s for Al-6wt.%Cu alloy. On the other hand, the  $V_L$  and  $T_R$  values have changed from 0.47 mm/s to 1.65 mm/s and 0.44 K/s to 14.0 K/s, respectively, for Al-3wt.% Cu alloy;

2. The highest and lowest  $V_L$  and  $T_R$  values found for Al-3wt.% Cu and Al-wt.6%Cu alloys, respectively, have resulted as a consequence in  $\lambda_2$  lowest and highest values for the respective investigated alloys;

3. The resulting microstructures revealed by Scanning Electron Microscopy (SEM) at the analyzed positions (10 mm and 70 mm from cooled interface) have shown the presence of aluminum rich matrix ( $\alpha$ -Al) and  $Al_2Cu$  intermetallic phase;

4. It was observed that due to  $V_L$  and  $T_R$  lower values and, consequently,  $\lambda_2$  higher values at the position 70 mm, the  $Al_2Cu$  intermetallic phase has been more susceptible to the action of electrochemical corrosion phenomena;

5. The analysis of experimental open circuit potential and polarization curves obtained for positions 10 mm and 70 mm have allowed to observe a more anodic behavior at the position 10 mm, which is closest to the metal-mold interface, providing at this position higher and smaller corrosion potentials ( $E_{CORR}$ ) and corrosion current ( $I_{CORR}$ ) values, respectively, compared with those obtained at the position 70 mm;

6. It was found for both investigated positions, 10 mm and 70 mm, that after the first 20 minutes of test, a growing profile of  $H_2$  release volume with time being more relevant at the position 70 mm, which provided greater mass loss, and, consequently, provided a  $H_2$  released total volume ( $H_2Vol$ ) at this position, that is, it has been demonstrated greater weight loss under conditions of  $V_L$  and  $T_R$  lower values, where  $\lambda_2$  is greater;

7. For the  $\lambda_2$  value = 40  $\mu m$  it was possible to observe that Al-6wt.%Cu alloy has a higher ECR than Al-3wt.%Cu alloy.

#### ACKNOWLEDGEMENTS

The authors gratefully acknowledge the provision of additional funds supplied by Federal Institute of Education, Science and Technology of Pará (IFPA), Federal University of Pará (UFPA), Brazilian Research Council (CNPq - grants 472745/2013-1 and 308784/2014-6), and Coordination of Superior Level Staff Improvement (CAPES), Brazil.

#### References

1. D.R. Poirier, K. Yeun and A.C. Maples, *Metall. Mater. Trans. A*, 18 (1987) 1987.
2. C.T. Rios and R. Caram, *J. Cryst. Growth*, 174 (1997) 65.
3. S. Engin, U. Büyük and N. Maraşlı, *J. Alloys Compd.*, 660 (2016) 23.
4. T.A. Costa, A.L. Moreira, D.J. Moutinho, M. Dias, I.L. Ferreira, J.E. Spinelli, O.L. Rocha and A. Garcia, *Mater. Sci. Technol.*, 31 (2015) 1103.
5. M. Gündüz and E. Çadirli, *Mater. Sci. Eng., A*, 327 (2002) 167.

6. D.B. Carvalho, E.C. Guimarães, A.L. Moreira, D.J. Moutinho, J.M. Dias Filho and O.L. Rocha, *Mater. Res.*, 16 (2013) 874.
7. L.G. Gomes, D.J. Moutinho, I. L. Ferreira, O.L. Rocha and A. Garcia, *Appl. Mech. Mater.*, 719-720 (2015) 102.
8. O.L. Rocha, C.A. Siqueira and A. Garcia, *Metall. Mater. Trans. A*, 34 (2003) 995.
9. M.D. Peres, C.A. Siqueira and A. Garcia, *J. Alloys Compd.*, 381 (2004) 168.
10. W.R. Osório, J.E. Spinelli, I.L. Ferreira and A. Garcia, *Electrochim. Acta*, 52 (2007) 3265.
11. W.R. Osório, L.C. Peixoto, D.J. Moutinho., L.G. Gomes, I.L. Ferreira and A. Garcia, *Mater. Des.*, 32 (2011) 3832.
12. W.R. Osório, D.J. Moutinho, L.C. Peixoto, I.L. Ferreira and A. Garcia, *Electrochim. Acta*, 56 (2011) 8412.
13. J.N. Silva, D.J. Moutinho, A.L. Moreira, I.L. Ferreira and O.L. Rocha, *J. Alloys Compd.*, 478 (2009) 358.
14. W.R. Osório, C.A. Siqueira, C.A. Santos and A. Garcia, *Int. J. Electrochem. Sci.*, 6 (2011) 6275.
15. W.R. Osório, C.M. Freire, R. Caram and A. Garcia, *Electrochim. Acta*, 77 (2012) 189.
16. H.O. Santos, F.M. Reis, C.T. Kuniyoshi, J.L. Rossi and I. Costa, *Mater. Res.*, 8 (2005) 155.
17. T.A. Costa, E.S. Freitas, M. Dias, C. Brito, N. Cheung and A. Garcia, *J. Alloys Compd.*, 653 (2015) 243.
18. A.S. Barros, I.A. Magno, F.A. Souza, C.A. Mota, A.L. Moreira, M.A. Silva and O.L. Rocha, *Met. Mater. Int.*, 21 (2015) 429.
19. E. Çadirli, *Met. Mater. Int.*, 19 (2013) 411.
20. D. Bouchard and J.S. Kirkaldy, *Metall. Mater. Trans. B*, 28 (1997) 651.
21. A.E. Ares, L.M. Gassa, S.F. Gueijman and C.E. Schvezov, *J. Cryst. Growth*, 310 (2008) 1355.
22. A.E. Ares, L.M. Gassa, C.E. Schvezov and M.R. Rosenberger, *Mater. Chem. Phys.*, 136 (2012) 394.
23. W.R. Osório, D.M. Rosa and A. Garcia, *Electrochim. Acta*, 56 (2011) 8457.
24. W.R. Osório, L.R. Garcia, L.C. Peixoto and A. Garcia, *Mater. Des.*, 32 (2011) 4763.
25. W.R. Osório, D.M. Rosa, L.C. Peixoto and A. Garcia, *J. Power Sources*, 196 (2011) 6567.
26. W.R. Osório, L.C. Peixoto and A. Garcia, *Int. J. Electrochem. Sci.*, 6 (2011) 1522.
27. W.R. Osório, D.M. Rosa and A. Garcia, *Electrochim. Acta*, 56 (2011) 8457.
28. W.R. Osório, J.E. Spinelli, C.R.M. Afonso, L.C. Peixoto and A. Garcia, *Electrochim. Acta*, 56 (2011) 8891.
29. C. Brito, T. Vida, E. Freitas, N. Cheung and J.E. Spinelli, *J. Alloys Compd.*, 673 (2016) 220.
30. ASTM G 59-97, Standard Test Method for Conducting Potentiodynamic Polarization Resistance Measurements, Annual Book of ASTM Standards, vol. 03.02, 2014.